Fatigue & Fracture of Engineering Materials & Structures

WILEY

FFEMS Fatigue & Fracture of Engineering Materials & Structures

ORIGINAL ARTICLE OPEN ACCESS

Static Assessment of Hybrid Double-Lap Bolted Joints With Additively Manufactured 316L Plates

Hasan Almuhanna[1] | Giacomo Torelli[1] | Luca Susmel[2]

[1]School of Mechanical, Aerospace and Civil Engineering, The University of Sheffield, Sheffield, UK | [2]School of Engineering and Built Environment, Sheffield Hallam University, Sheffield, UK

Correspondence: Luca Susmel (l.susmel@shu.ac.uk)

Received: 13 October 2025 | **Revised:** 11 January 2026 | **Accepted:** 27 January 2026

Keywords: design estimations | hybrid bolted joints | selective laser melting | static failure | wire arc additive manufacturing

ABSTRACT

The present study examines the static response and evaluates the accuracy of design standards and selected literature-based design criteria in estimating the load capacity of the inner plates of double-lap shear bolted connections in single- and double-bolt configurations. The analysis is based on 70 experiments previously reported by the authors, including conventional and additively manufactured inner plates produced by wire arc additive manufacturing and selective laser melting. While additively manufactured plates exhibited load capacities comparable to conventional plates, they generally showed reduced ductility. Experimental load capacities are compared against the European standards EC3-1-8 and EC3-1-4 and the American standard AISC 370. Although originally developed for carbon steel, EC3-1-8 provided the most accurate estimations, whereas EC3-1-4 and AISC 370 consistently overestimated the load capacity. Literature-based equations showed the closest agreement, highlighting limitations in current standards for additively manufactured bolted plates.

1 | Introduction

Additive manufacturing (AM) is redefining structural engineering by enabling the production of complex, optimized geometries through layer-by-layer fabrication guided by digital design models [1]. The feasibility of this technology was demonstrated by the successful construction of the first full-scale AM footbridge, fabricated using grade 308LSi austenitic stainless steel wire via wire arc additive manufacturing (WAAM). The bridge underwent extensive material, component, and structural testing and was validated under serviceability design loads, showcasing the potential of AM for large-scale structural applications [2]. As the technology is rapidly advancing, especially in the use of metals such as steels and stainless steels, a growing body of research is focusing on reduced-scale specimens to address open questions related to mechanical performance, surface quality, and structural integrity [3].

Several experimental studies have examined the mechanical performance of WAAM plates integrated as a component in bolted connections in both single- and double-lap shear testing arrangements, covering metals including carbon steel, duplex stainless steel, and austenitic stainless steel [4–10]. These investigations have identified a range of failure modes such as shear-out, net-section tension, bearing, out-of-plane curling, and an unexpected failure of end-splitting. These studies also show that the structural response is influenced by WAAM characteristics including material anisotropy, extraction direction, and surface conditions.

Among the studies investigating WAAM-produced bolted connections, four have specifically focused on double-lap shear arrangements and evaluated the accuracy of various established design specifications. WAAM carbon steel connections were examined in [5], covering several geometrical combinations

Summary

- Hybrid AM plates show reduced ductility versus conventional plates in shear-bolted joints.
- Diagonally extracted WAAM plates exhibit improved deformation response.
- EC3-1-8 predicts load capacity more accurately than stainless-steel-specific standards.
- Literature-based equations give the closest match to experimental failure loads.

and two distinct nominal plate thicknesses. The study in [5] assessed several design provisions; among these, the previous edition of Eurocode BS EN 1993-1-8 for steel joints [11] yielded a mean experimental-to-estimated resistance ratio of 1.11 with a coefficient of variation (COV) of 0.073 [5], where the COV, defined as the standard deviation divided by the mean, indicates good agreement with the test results. A slightly higher mean ratio of 1.15 with greater variability (COV = 0.13) using the same previous edition of Eurocode BS EN 1993-1-8 provision was observed in [6], which also studied WAAM carbon steel. Although the average resistance was estimated reasonably well, the higher COV indicates reduced reliability. The work in [7] extended this research by testing thick WAAM carbon steel plates (7.9–9.3 mm in thickness) and employed the updated Eurocode BS EN 1993-1-8 provision for steel joints [12], reporting a mean ratio of 1.11 and a lower COV of 0.07, which is comparable to the results reported in [5], despite the use of an updated Eurocode provision. Meanwhile, experiments on WAAM-produced 316L stainless steel connections were conducted in [8], demonstrating that the American standard ANSI/AISC 370 [13] yielded a higher mean ratio of 1.45 but with relatively low variability (COV = 0.088). Collectively, these studies illustrate the varying degrees of conservatism and precision when applying traditional steel design codes to WAAM-manufactured steel connections.

While both WAAM and selective laser melting (SLM) have been widely studied in the context of 316L stainless steel, most research on SLM-produced 316L has focused on microstructural characteristics and basic material properties such as anisotropy, porosity, and plain material mechanical behavior [14–17]. However, a recent study has examined its structural performance in bolted connections, and it focused on conditions following fire exposure [18]. As a result, there remains limited data on how SLM 316L stainless steel behaves in structural applications or whether its performance aligns with established design estimations. This presents an opportunity to assess the connection-level capacity of SLM plates against existing design codes.

Despite growing interest in the structural use of additive manufacturing, the design of WAAM stainless steel bolted connections remains underexplored. As mentioned above, only a limited number of studies have investigated both single- and double-lap WAAM and SLM 316L stainless steel bolted connections, while most existing research has focused on carbon steels. Therefore, the existing research is insufficient to assess the reliability of design standards and literature-based equations for such additively manufactured plates. The present study provides new insight by experimentally evaluating both single- and double-bolted configurations produced using SLM and WAAM, considering variations in geometry, print direction, and surface condition. Their performance is then compared against established design standards and proposed bearing strength equations from recent literature.

2 | Reference Experiments

The 316L stainless steel specimens examined in this study include conventionally manufactured reference plates, as well as plates produced using two additive manufacturing methods: SLM and WAAM. The fabrication procedures are described in a previous study from the authors [19], where the same specimens were used to investigate failure modes. In the present work, the focus is on examining the load–displacement response and evaluating both codified design provisions and equations developed in the literature for estimating the failure mechanism of the bolted connections. WAAM plates were produced using a robotic welding system with 316L wire under argon shielding, extracted from tubular builds via wire electrical discharge machining (EDM). SLM plates were fabricated using a laser-based powder bed system in an inert gas atmosphere and printed directly to the final dimensions. The mechanical properties of the parent materials, summarized in Table 1, were also reported in the previous study [19], where the strength properties of these materials were obtained from coupon testing.

Experimental testing employed a double-lap shear setup (Figure 1), conducted on a Shimadzu universal testing machine equipped with a 300-kN load cell. Displacement-controlled loading was applied at a constant rate of 1 mm/min until failure. The

TABLE 1 | Mechanical properties of CON and AM 316L stainless steel coupons [19].

Designation	Modulus of elasticity, E (GPa)	Offset yield stress, $f_{y,0.2}$ (MPa)	Ultimate stress, f_u (MPa)
CON	184	488	667
WAAM-M-0°	143	288	521
WAAM-M-45°	185	324	552
WAAM-M-60°	160	297	530
WAAM-M-90°	103	281	562
WAAM-AB-0°	124	278	493
WAAM-AB-45°	119	282	544
WAAM-AB-60°	139	323	566
WAAM-AB-90°	91	273	493
SLM-AB-0°	160	520	627
SLM-AB-45°	126	422	562
SLM-AB-90°	120	419	554

setup was configured to promote failure in the thinner inner plates, while the thicker outer plates were designed to remain elastic and reduce secondary bending effects. Two primary configurations were investigated, comprising inner plates with either single or double bolt holes. Within each configuration, variations in geometrical variables presented in Figure 1, including end distance, e_1, edge distance, e_2, and pitch distance, p, were used to promote different failure modes, namely shear-out (SO), edge bearing (EB), net-section tension (NST), and block tearing (BT), the latter occurring in double-bolt configurations. Due to the ductile behavior of 316L stainless steel, stress concentrations associated with bolt-hole interaction and the resulting large plastic deformation led most inner plates to exhibit a combination of failure modes, typically involving precursor EB failure followed by a governing partial or complete SO, NST, or BT, with only the final governing mode reported here, as shown in Figure 2 [19].

The AM plates varied in build orientation: for SLM, this referred to the direction of printing, whereas for WAAM, it denoted the extraction direction. Specifically, the angle printing direction, θ, is here defined as the angle between the extraction/printing direction and the direction of applied load. The tested inner plates included: conventionally manufactured plates (CON); SLM-produced plates tested in the as-built (SLM-AB) and machined (SLM-M) conditions; and WAAM-produced plates tested in the machined (WAAM-M) and as-built (WAAM-AB) conditions. All CON, SLM-M, SLM-AB, and WAAM-M plates had a uniform thickness, t of 2 mm. In the case of WAAM-M plates, the term M indicates that the plates were machined down to 2 mm to remove surface undulations. For SLM-M, M denotes only the removal of the rough surface, as the as-built thickness was already close to 2 mm. WAAM-AB plates were fabricated with an average $t = 5.3$ mm due to printing constraints. As reported in [19], no variation in failure modes was expected compared

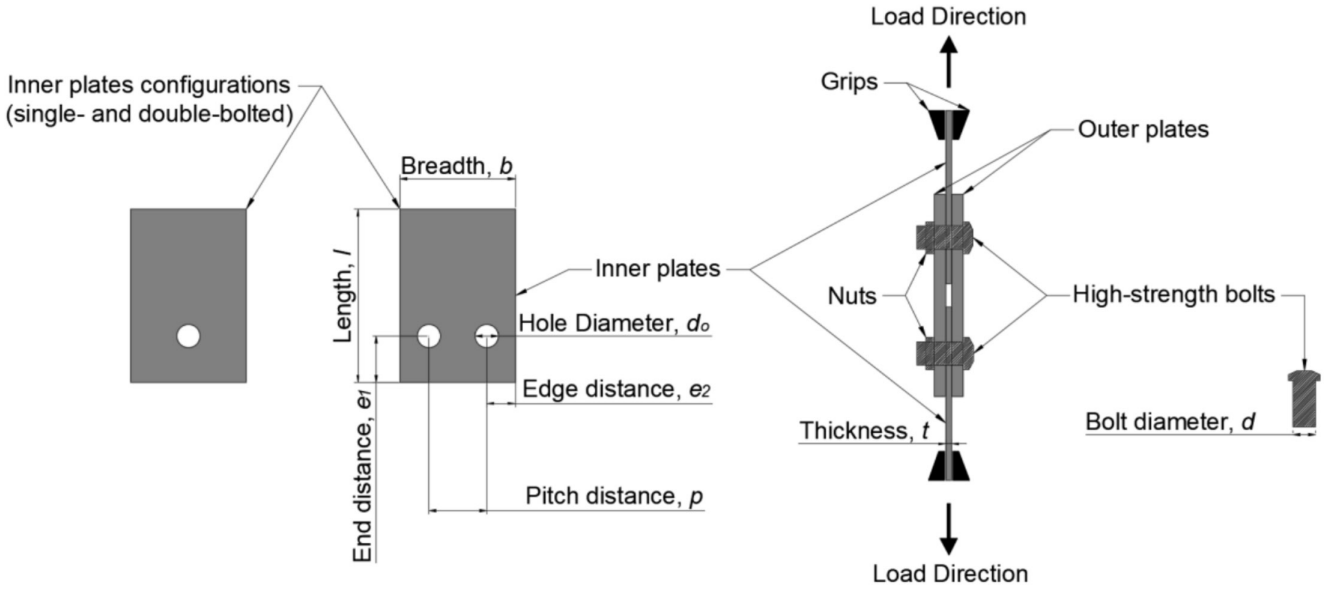

FIGURE 1 | Test setup for double-lap shear bolted connections.

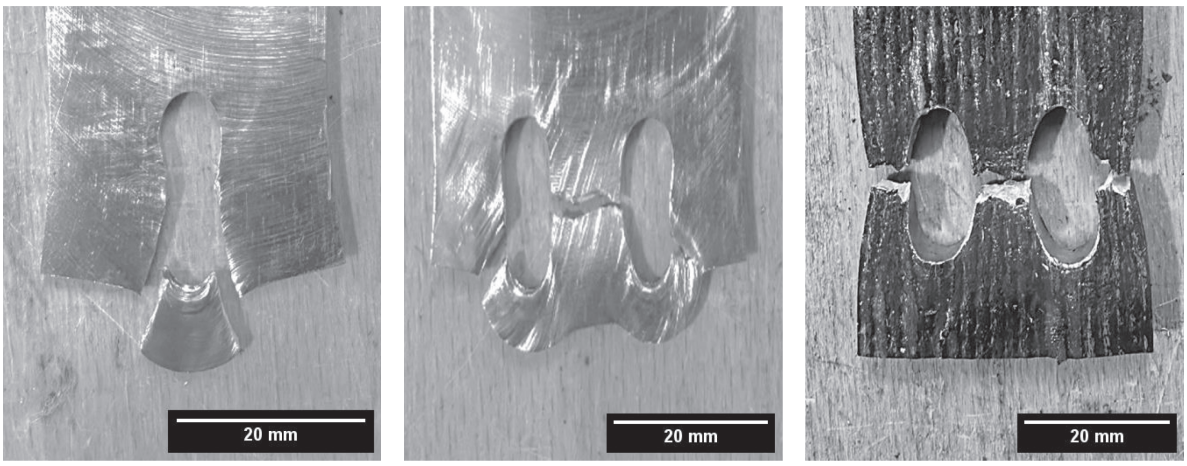

FIGURE 2 | Representative governing failure modes observed in double-bolted configuration plates: (a) and (b) correspond to WAAM machined plates exhibiting SO and BT failures, respectively; (c) shows a WAAM as-built plate with NST failure [19].

TABLE 2 | Tested specimens—single-bolt configuration [19].

Designation	Bolt type	Bolt grade	Hole diameter, d_o	Thickness, t (mm)	End distance, e_1 (mm)	Edge distance, e_2 (mm)	Breadth, b (mm)
IP1-1-CON	M6	10.9	6.6	2	14	15	30
IP1-2-CON	M6	10.9	6.6	2	13	15	30
IP1-3-CON	M6	10.9	6.6	2	11	15	30
IP1-4-CON	M6	10.9	6.6	2	8	15	30
IP1-5-CON	M6	10.9	6.6	2	15	8	16
IP1-1-WAAM-M-0°	M6	10.9	6.6	2	14	15	30
IP1-1-WAAM-M-45°	M6	10.9	6.6	2	14	15	30
IP1-1-WAAM-M-60°	M6	10.9	6.6	2	14	15	30
IP1-1-WAAM-M-90°	M6	10.9	6.6	2	14	15	30
IP1-2-WAAM-M-0°	M6	10.9	6.6	2	14	15	30
IP1-2-WAAM-M-45°	M6	10.9	6.6	2	14	15	30
IP1-2-WAAM-M-60°	M6	10.9	6.6	2	14	15	30
IP1-2-WAAM-M-90°	M6	10.9	6.6	2	14	15	30
IP1-3-WAAM-M-0°	M6	10.9	6.6	2	11	15	30
IP1-4-WAAM-M-0°	M6	10.9	6.6	2	8	15	30
IP1-1-WAAM-AB-0°	M8	12.9	8.4	5.4	14	15	30
IP1-2-WAAM-AB-0°	M8	12.9	8.4	5.4	13	15	30
IP1-2-WAAM-AB-45°	M8	12.9	8.4	5.3	13	15	30
IP1-2-WAAM-AB-60°	M8	12.9	8.4	5.2	13	15	30
IP1-2-WAAM-AB-90°	M8	12.9	8.4	5.2	13	15	30
IP1-3-WAAM-AB-0°	M8	12.9	8.4	5.3	11	15	30
IP1-4-WAAM-AB-0°	M8	12.9	8.4	5.4	8	15	30
IP1-5-WAAM-AB-0°	M8	12.9	8.4	5.2	15	8	16
IP1-5-WAAM-AB-45°	M8	12.9	8.4	5.4	15	8	16
IP1-5-WAAM-AB-60°	M8	12.9	8.4	5.3	15	8	16
IP1-5-WAAM-AB-90°	M8	12.9	8.4	5.3	15	8	16
IP1-1-SLM-M-0°	M6	10.9	6.6	2	14	15	30
IP1-1-SLM-AB-0°	M6	10.9	6.6	2	14	15	30
IP1-2-SLM-AB-0°	M6	10.9	6.6	2	13	15	30
IP1-2-SLM-AB-45°	M6	10.9	6.6	2	13	15	30
IP1-2-SLM-AB-90°	M6	10.9	6.6	2	13	15	30
IP1-5-SLM-AB-0°	M6	10.9	6.6	2	15	8	16
IP1-5-SLM-AB-45°	M6	10.9	6.6	2	15	8	16
IP1-5-SLM-AB-90°	M6	10.9	6.6	2	15	8	16

TABLE 3 | Tested specimens—double-bolt configurations [19].

Designation	Bolt type	Bolt grade	Hole diameter, d_o	Thickness, t (mm)	End distance, e_1 (mm)	Edge distance, e_2 (mm)	Pitch distance, p (mm)	Breadth, b (mm)
IP2-1-CON	M6	10.9	6.6	2	12	12	16	40
IP2-2-CON	M6	10.9	6.6	2	11	12	16	40
IP2-3-CON	M6	10.9	6.6	2	8.2	12	16	40
IP2-4-CON	M6	10.9	6.6	2	8	12	16	40
IP2-5-CON	M6	10.9	6.6	2	7	12	16	40
IP2-6-CON	M6	10.9	6.6	2	16	8	24	40
IP2-7-CON	M6	10.9	6.6	2	15	11	18	40
IP2-1-WAAM-M-0°	M6	10.9	6.6	2	12	12	16	40
IP2-1-WAAM-M-45°	M6	10.9	6.6	2	12	12	16	40
IP2-1-WAAM-M-60°	M6	10.9	6.6	2	12	12	16	40
IP2-1-WAAM-M-90°	M6	10.9	6.6	2	12	12	16	40
IP2-2-WAAM-M-0°	M6	10.9	6.6	2	11	12	16	40
IP2-3-WAAM-M-0°	M6	10.9	6.6	2	8.2	12	16	40
IP2-3-WAAM-M-45°	M6	10.9	6.6	2	8.2	12	16	40
IP2-3-WAAM-M-60°	M6	10.9	6.6	2	8.2	12	16	40
IP2-3-WAAM-M-90°	M6	10.9	6.6	2	8.2	12	16	40
IP2-4-WAAM-M-0°	M6	10.9	6.6	2	8	12	16	40
IP2-5-WAAM-M-0°	M6	10.9	6.6	2	7	12	16	40
IP2-7-WAAM-M-0°	M6	10.9	6.6	2	8.2	12	16	40
IP2-2-WAAM-AB-0°	M8	12.9	8.4	5.5	11	12	16	40
IP2-3-WAAM-AB-0°	M8	12.9	8.4	5.6	8.2	12	16	40
IP2-3-WAAM-AB-45°	M8	12.9	8.4	5.2	8.2	12	16	40
IP2-3-WAAM-AB-60°	M8	12.9	8.4	5.5	8.2	12	16	40
IP2-3-WAAM-AB-90°	M8	12.9	8.4	5.3	8.2	12	16	40

(Continues)

TABLE 3 | (Continued)

Designation	Bolt type	Bolt grade	Hole diameter, d_o	Thickness, t (mm)	End distance, e_1 (mm)	Edge distance, e_2 (mm)	Pitch distance, p (mm)	Breadth, b (mm)
IP2-4-WAAM-AB-0°	M8	12.9	8.4	5.0	8	12	16	40
IP2-5-WAAM-AB-0°	M8	12.9	8.4	5.3	7	12	16	40
IP2-6-WAAM-AB-0°	M8	12.9	8.4	5.4	16	8	24	40
IP2-6-WAAM-AB-45°	M8	12.9	8.4	5.0	16	8	24	40
IP2-6-WAAM-AB-60°	M8	12.9	8.4	5.3	16	8	24	40
IP2-6-WAAM-AB-90°	M8	12.9	8.4	5.0	16	8	24	40
IP2-7-WAAM-AB-0°	M8	12.9	8.4	5.4	8.2	12	16	40
IP2-7-SLM-M-0°	M6	10.9	6.6	2	15	11	18	40
IP2-6-SLM-AB-0°	M6	10.9	6.6	2	16	8	24	40
IP2-6-SLM-AB-45°	M6	10.9	6.6	2	16	8	24	40
IP2-6-SLM-AB-90°	M6	10.9	6.6	2	16	8	24	40
IP2-7-SLM-AB-0°	M6	10.9	6.6	2	15	11	24	40

to their WAAM-M counterparts, although a significant increase in load capacity was observed with increased thickness. Tables 2 and 3 give an overview of the tested specimens with their unique designation [19]. For example, IP1-1-WAAM-M-0° refers to configuration 1-1, featuring inner plates produced via WAAM. M indicates that the plates were machined, while 0° denotes the extraction or printing direction, θ against the applied load.

3 | Comparison of Global Load–Displacement Response Across Manufacturing Methods

In addition to the interpretation of the failure modes and crack behavior of the inner plates previously reported in [19], this section presents further analysis of the global load–displacement response of the tested connections. The load–displacement curves provide direct insight into the ductility of additively manufactured (AM) plates relative to their conventional (CON) counterparts. Since ductility is a key design parameter alongside strength, these curves provide a more complete understanding of the mechanical response of the connections before assessing the code-based estimations.

A comparative assessment of the 2-mm-thick plates based on the global load–displacement curves across CON and AM tests can be seen in Figure 3a–e for the single-bolt configuration and Figure 4a–g for double-bolt configuration. The comparison reveals noticeable differences between the CON and AM specimens. Based on these figures, the load capacity of AM plates is broadly comparable to that of CON plates, with only minor variations observed. However, a clear difference is seen in terms of displacement at failure, δ, where AM plates consistently failed at lower δ values. For instance, in Figure 3a, IP1-1-CON reached a total $\delta = 19.5$ mm, whereas the highest displacements for WAAM-M and SLM-M and SLM-AB were $\delta = 12.8$, 11.2, and 9.2 mm respectively. This trend is also evident in the double-bolt configurations (Figure 4a–g), where CON plates again demonstrated greater displacement before failure. This indicates that AM plates have a detrimental effect in terms of elongation before failure, and they are less ductile than CON. Nevertheless, AM plates exhibited a steeper initial slope compared to CON plates, indicating enhanced connection stiffness. This could be attributed to differences in bolt-plate interaction, including increased friction due to surface roughness in SLM plates and inherently higher bearing stiffness of both WAAM and SLM plates. This also suggests that AM plates undergo less elastic deformation before entering the plastic zone, further supporting the observation that they are less ductile and potentially more brittle than their CON counterparts. Additionally, the extraction orientation of $\theta = 45°$ and 60° in WAAM-M appeared to influence ductility, as

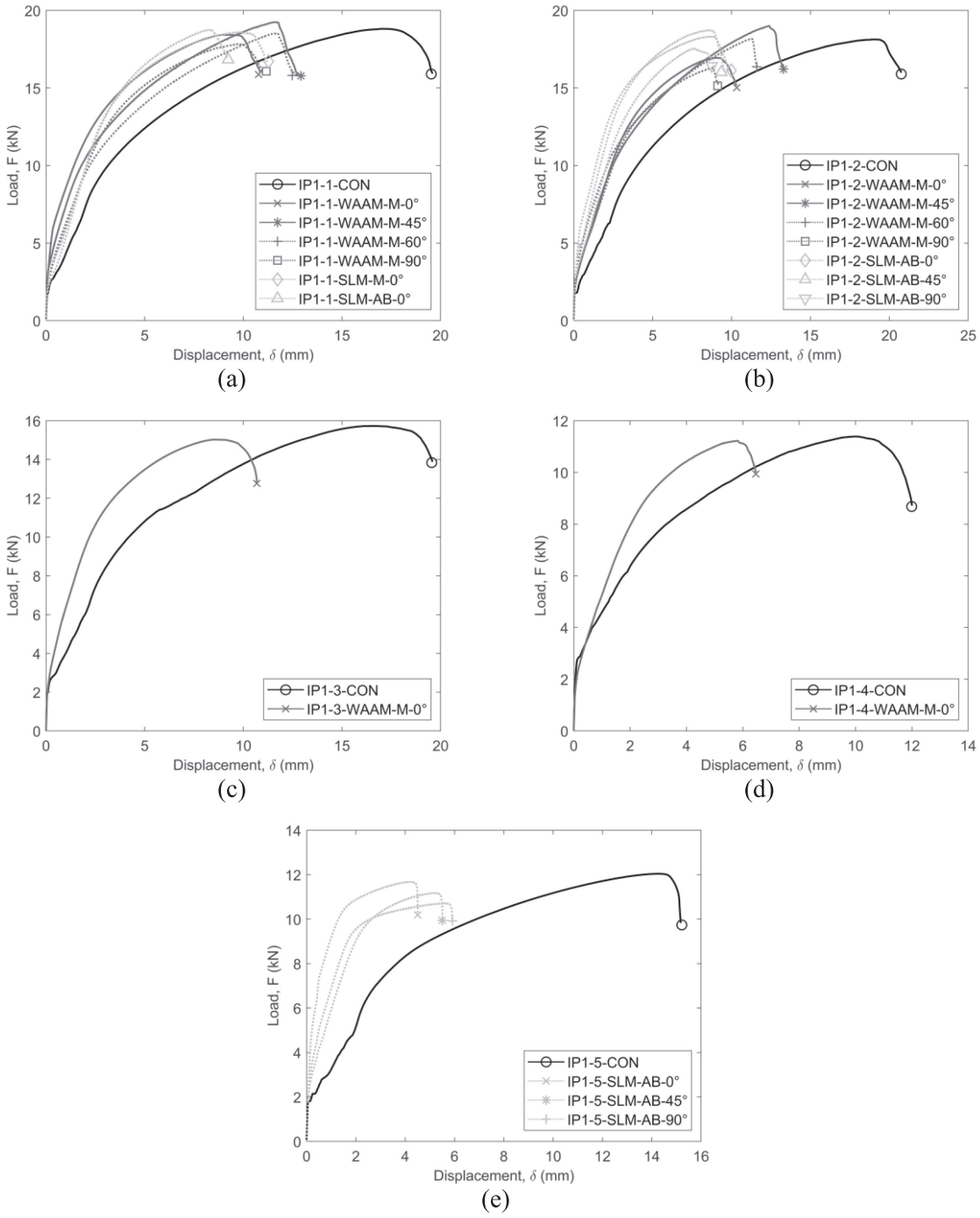

FIGURE 3 | Load–displacement curves for single-bolt configurations with a consistent $t = 2$ mm: comparison between CON and AM plates.

these orientations exhibited slightly improved elongation. This observation aligns with coupon testing observed in [19], which showed that the diagonal printing orientation is beneficial to ductility. This further indicates that, despite the undulations being removed from the surface, the influence of the printing process persisted at the microstructural level, suggesting that the underlying grain structure and layer orientation contribute to this behavior. For SLM tests, no clear consistency in behavior was observed across different θ and surface conditions. This may imply that these variables have a less significant effect on mechanical performance in SLM compared to WAAM, where printing orientation and surface condition exhibit a more pronounced influence.

Beyond differences related to manufacturing extraction/print direction, θ, the influence of geometrical variables on load-bearing capacity and displacement was also evident. A decrease in end distance, e_1 from 14 to 8 mm for single-bolt configurations and from 14 to 8 mm for double-bolt configurations led to a noticeable reduction in both load capacity and ultimate displacement before failure. This trend was observed across all AM and CON plates, where specimens with shorter

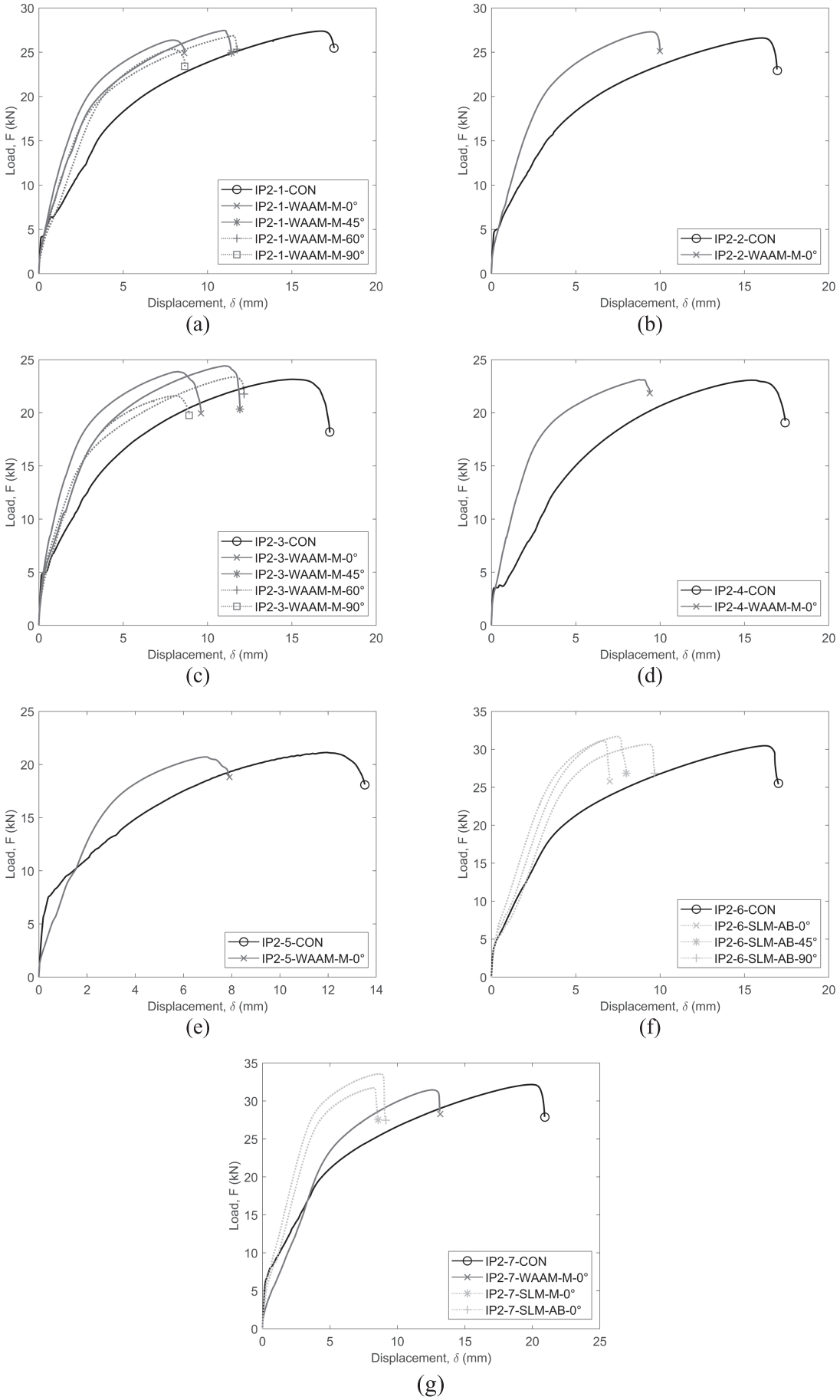

FIGURE 4 | Load–displacement curves for double-bolt configurations with a consistent $t = 2$ mm: comparison between CON and AM plates.

end distances exhibited earlier failure. Furthermore, the lower breadth, b, value in IP1-5 (Figure 3e) resulted in a significant reduction in load capacity, despite e_1 having an adequate value of 15 mm. In contrast, IP2-7 (Figure 4g), which had large e_1, pitch distance, p, and sufficient edge distance, e_2, demonstrated improved overall performance. While these values were intentionally selected to ensure specific failure modes in the tested plates, the observed variations highlight the importance of adhering to design standard threshlds to achieve optimal structural performance.

In the case of WAAM-AB, the results for both single- and double-bolt configurations are shown in Figures 5a–e and 6a–f, respectively. The curves differ markedly from those of the other specimens due to a significant increase in load-bearing capacity, primarily attributed to increased thickness, t. Despite surface undulations causing local variation in thickness, t, its overall increase played a key role in enhancing plate performance. Furthermore, comparisons of extraction direction in Figures 5b,e and 6b,e reinforced that a diagonal orientation (e.g., $\theta = 45°$ and 60°) is beneficial, noting that the performance of IP1-2-WAAM-AB-90° in Figure 4b did not follow this trend and was deemed to be an outlier.

4 | Evaluation of Design Estimations

4.1 | General

This section presents the equations used to estimate the design loads of double-lap shear bolted connections, as provided by the most commonly adopted design standards: BS EN 1993-1-8 [12], BS EN 1993-1-4 [20], and ANSI/AISC 370 [13], hereafter referred to as EC3-1-8, EC3-1-4, and AISC370, respectively. In addition to these standards, literature-based equations (LBE) specifically developed for AM bolted connections are also considered. All equations are applied using a strength-based criterion without the inclusion of partial safety factors, enabling

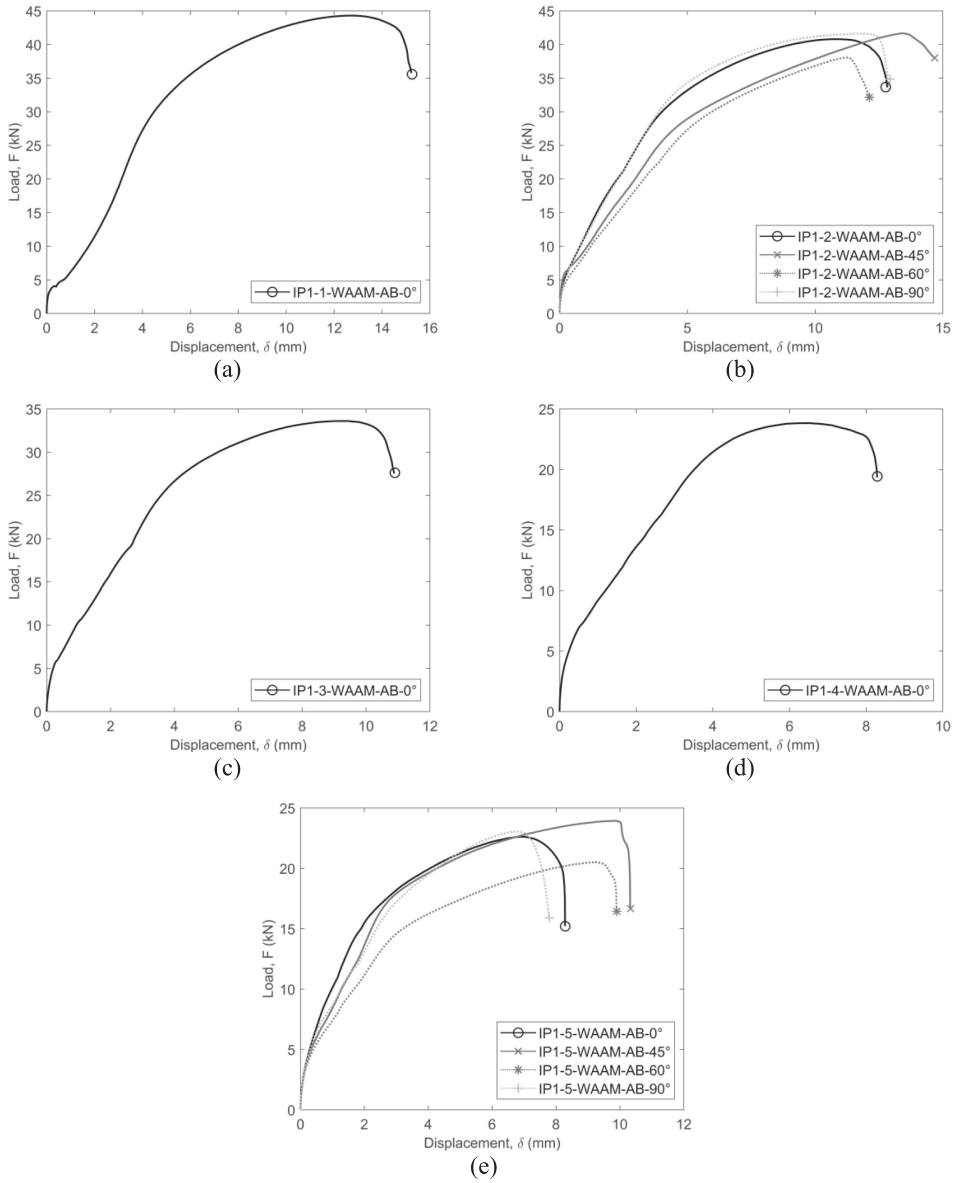

FIGURE 5 | Load–displacement curves for single-bolt WAAM-AB configurations with non-uniform t and larger d_o.

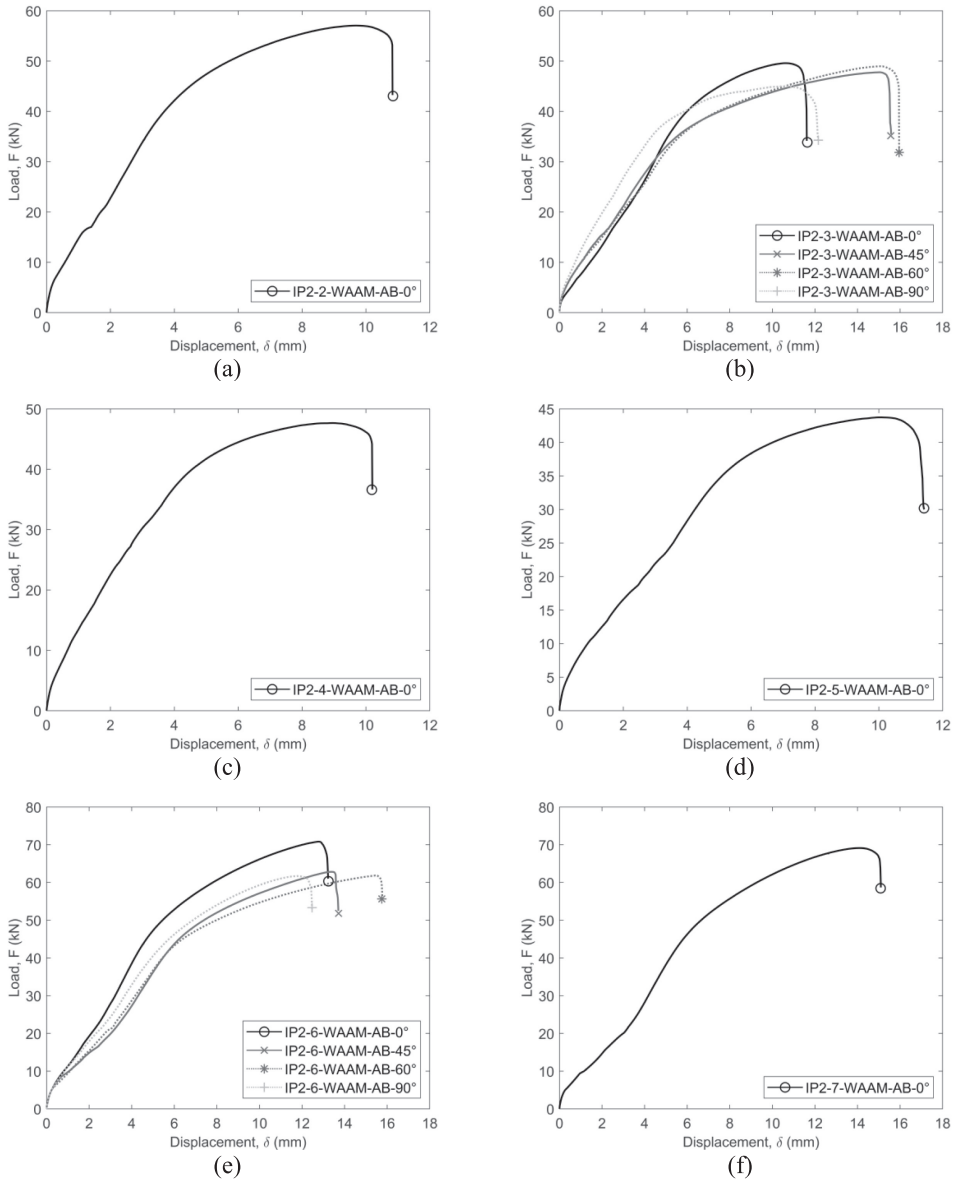

FIGURE 6 | Load–displacement curves for double-bolt WAAM-AB configurations with non-uniform t and larger d_o.

direct comparison with the experimental failure loads of CON and AM plates under controlled test conditions.

4.2 | EC3-1-8

The European standard EC3-1-8 [12], which is specified for carbon steel bolted connections, defines the design bearing resistance, $F_{b,EC3}$ to be calculated using Equation (1):

$$F_{b,EC3} = n_b k_m a_b f_u dt \tag{1}$$

where n_b is the number of bolts, k_m is a factor depends on the steel grade of the plate, f_u is the nominal material ultimate tensile strength of the plate, and a_b is taken as the minimum of three values: e_1 / d_o (associated with edge bearing), $3 \times f_{ub} / f_u$ (associated with bolt bearing), and 3 (calibration limit). The notation f_{ub} is the nominal ultimate tensile strength of the bolt. The smallest of these values reflects the governing bearing mode in the connection.

For calculating the design net-section tension resistance, EN 1993-1-8 [12] refers to Equations (2), (3), (4), (5), and (6):

$$F_{t,Rd} = min\left[F_{pl,EC3}; F_{n,EC3}\right] \tag{2}$$

$$F_{pl,EC3} = A_g f_y \tag{3}$$

$$F_{n,EC3} = kA_{net} f_u \tag{4}$$

$$A_{net} = A_g - \Delta A_{net} \tag{5}$$

$$\Delta A_{net} = n_b d_o t \tag{6}$$

As shown in Equation (2), the design net-section tension resistance, $F_{t,EC3}$, of the plate is the minimum value of two: the design plastic resistance of the gross cross-section, $F_{pl,EC3}$, or the design

TABLE 4 | Comparison between experimental results and design provision estimations [12, 13, 20] for the failure mechanisms of single-bolt configurations.

Designation	Experimental ultimate load, F_{Exp} (kN)	Governing failure mode	Design resistance to EC3-1-8, $F_{EC3-1-8}$ (kN)	Ratio to EC3-1-8, $\frac{F_{Exp}}{F_{EC3-1-8}}$	Failure mode (EC3-1-8)	Design resistance to EC3-1-4, $F_{EC3-1-4}$ (kN)	Ratio to EC3-1-4, $\frac{F_{Exp}}{F_{EC3-1-4}}$	Failure mode (EC3-1-4)	Design resistance to AISC370, $F_{AISC370}$ (kN)	Ratio to AISC370, $\frac{F_{Exp}}{F_{AISC370}}$	Failure mode (AISC370)
IP1-1-CON	18.8	SO	17.0	1.11	EB	14.1	1.33	EB	14.1	1.33	SO
IP1-1-WAAM-M-0°	18.4	SO	13.3	1.38	EB	11.1	1.66	EB	11.1	1.66	SO
IP1-1-WAAM-M-45°	19.2	SO	14.1	1.36	EB	11.7	1.64	EB	11.7	1.64	SO
IP1-1-WAAM-M-60°	18.5	SO	13.5	1.37	EB	11.2	1.65	EB	11.2	1.65	SO
IP1-1-WAAM-M-90°	17.8	SO	14.3	1.24	EB	11.9	1.50	EB	11.9	1.50	SO
IP1-1-WAAM-AB-0°	44.3	SO	35.5	1.25	EB	29.6	1.50	EB	29.6	1.50	SO
IP1-1-SLM-M-0°	18.5	SO	16.0	1.16	EB	13.3	1.39	EB	13.3	1.39	SO
IP1-1-SLM-AB-0°	18.7	SO	16.0	1.17	EB	13.3	1.41	EB	13.3	1.41	SO
IP1-2-CON	18.1	SO	15.8	1.15	EB	13.1	1.38	EB	13.1	1.38	SO
IP1-2-WAAM-M-0°	16.9	SO	12.3	1.37	EB	10.3	1.64	EB	10.3	1.64	SO
IP1-2-WAAM-M-45°	19.0	SO	13.0	1.46	EB	10.9	1.74	EB	10.9	1.74	SO
IP1-2-WAAM-M-60°	18.1	SO	12.5	1.45	EB	10.4	1.74	EB	10.4	1.74	SO
IP1-2-WAAM-M-90°	16.2	SO	13.3	1.22	EB	11.1	1.46	EB	11.1	1.46	SO
IP1-2-WAAM-AB-0°	40.8	SO	33.0	1.24	EB	27.5	1.48	EB	27.5	1.48	SO
IP1-2-WAAM-AB-45°	41.6	SO	35.7	1.17	EB	29.7	1.40	EB	29.7	1.40	SO

(Continues)

TABLE 4 | (Continued)

Designation	Experimental ultimate load, F_{Exp} (kN)	Governing failure mode	Design resistance to EC3-1-8, $F_{EC3-1-8}$ (kN)	Ratio to EC3-1-8, $\frac{F_{Exp}}{F_{EC3-1-8}}$	Failure mode (EC3-1-8)	Design resistance to EC3-1-4, $F_{EC3-1-4}$ (kN)	Ratio to EC3-1-4, $\frac{F_{Exp}}{F_{EC3-1-4}}$	Failure mode (EC3-1-4)	Design resistance to AISC370, $F_{AISC370}$ (kN)	Ratio to AISC370, $\frac{F_{Exp}}{F_{AISC370}}$	Failure mode (AISC370)
IP1-2-WAAM-AB-60°	38.0	SO	36.4	1.04	EB	30.4	1.25	EB	30.4	1.25	SO
IP1-2-WAAM-AB-90°	41.6	SO	31.7	1.31	EB	26.4	1.58	EB	26.4	1.58	SO
IP1-2-SLM-AB-0°	18.3	SO	14.8	1.24	EB	12.4	1.48	EB	12.4	1.48	SO
IP1-2-SLM-AB-45°	18.7	SO	13.3	1.41	EB	11.1	1.68	EB	11.1	1.68	SO
IP1-2-SLM-AB-90°	17.5	SO	13.1	1.34	EB	10.9	1.61	EB	10.9	1.61	SO
IP1-3-CON	15.7	SO	13.3	1.18	EB	11.1	1.41	EB	11.1	1.41	SO
IP1-3-WAAM-M-0°	15.0	SO	10.4	1.44	EB	8.7	1.72	EB	8.7	1.72	SO
IP1-3-WAAM-AB-0°	33.6	SO	27.4	1.23	EB	18.2	1.85	EB	22.8	1.47	SO
IP1-4-CON	11.3	SO	9.7	1.16	EB	8.1	1.40	EB	8.1	1.40	SO
IP1-4-WAAM-M-0°	11.2	SO	7.6	1.47	EB	6.3	1.78	EB	6.3	1.78	SO
IP1-4-WAAM-AB-0°	23.8	SO	20.3	1.17	EB	13.5	1.76	EB	16.6	1.43	SO
IP1-5-CON	12.0	NST	12.5	0.96	NST	12.5	0.96	NST	12.5	0.96	NST
IP1-5-WAAM-AB-0°	22.6	NST	19.5	1.16	NST	19.5	1.16	NST	19.5	1.16	NST
IP1-5-WAAM-AB-45°	23.9	NST	22.3	1.07	NST	22.3	1.07	NST	22.3	1.07	NST
IP1-5-WAAM-AB-60°	20.5	NST	22.8	0.90	NST	22.8	0.90	NST	22.8	0.90	NST

(Continues)

TABLE 4 | (Continued)

Designation	Experimental ultimate load, F_{Exp} (kN)	Governing failure mode	Design resistance to EC3-1-8, $F_{EC3-1-8}$ (kN)	Ratio to EC3-1-8, $\frac{F_{Exp}}{F_{EC3-1-8}}$	Failure mode (EC3-1-8)	Design resistance to EC3-1-4, $F_{EC3-1-4}$ (kN)	Ratio to EC3-1-4, $\frac{F_{Exp}}{F_{EC3-1-4}}$	Failure mode (EC3-1-4)	Design resistance to AISC370, $F_{AISC370}$ (kN)	Ratio to AISC370, $\frac{F_{Exp}}{F_{AISC370}}$	Failure mode (AISC370)
IP1-5-WAAM-AB-90°	23.0	NST	19.9	1.16	NST	19.9	1.16	NST	19.9	1.16	NST
IP1-5-SLM-AB-0°	11.6	NST	11.8	0.98	NST	11.8	0.98	NST	11.8	0.98	NST
IP1-5-SLM-AB-45°	11.1	NST	10.6	1.05	NST	10.6	1.05	NST	10.6	1.05	NST
IP1-5-SLM-AB-90°	10.7	NST	10.4	1.03	NST	10.4	1.03	NST	10.4	1.03	NST

ultimate resistance of the net cross-section, $F_{n,EC3}$. Equation (3) is used to calculate $F_{pl,EC3}$, where A_g is the cross-sectional area of the plate and f_y is the nominal yield strength of the inner plate material. To calculate $F_{u,EC3}$, Equation (4) is applied, considering that k is a value depends on the hole fabrication method, and A_{net} is the net cross-sectional area. A_{net} is obtained using Equation (5) where ΔA_{net} represents the section area deducted due to the presence of hole/s. The value of ΔA_{net} can be directly calculated by using Equation (6).

The EN 1993-1-8 standard [12] further recommends applying Equation (7) to estimate the design block shear resistance, $F_{eff,EC3}$, for plates with two or more bolts.

$$F_{eff,EC3} = \left(A_{nt} f_u\right) + min\left[\frac{A_{gv} f_y}{\sqrt{3}}; \frac{A_{nv} f_u}{\sqrt{3}}\right] \tag{7}$$

The terms A_{nt}, A_{gv}, and A_{nv} refer to the net area subjected to tension, the gross area subjected to shear, and the net area subjected to shear, respectively.

4.3 | EC3-1-4

EC3-1-4 [20] refers to EC3-1-8 [12] for the general design of bolted connections, including lap-shear configurations. That said, there is an adjustment to the bearing resistance equation, as EC3-1-4 [20] introduces specific provisions for stainless steel. The bearing resistance for stainless steel, $F_{b,EC3*}$ is determined using Equation (8) with specific considerations defined in EC3-1-4 [20].

$$F_{b,EC3*} = n_b a_b k_1 f_u dt \tag{8}$$

The notation a_b represents the bearing coefficient in the direction of the load transfer, while k_1 is the bearing coefficient in the direction perpendicular to the load transfer. The values of k_1 and a_b for edge bolts are calculated depending on the thickness of the plate and the chosen failure criterion. Since these tests aim to estimate failure at the ultimate state, the strength criterion is selected, and its corresponding a_b and k_1 values are calculated using Equations (9) and (10). The lowest value of a_b is the value associated with the bearing type that occurs in the connections.

$$a_b = min\left[2.5; \frac{5e_1}{6d_o}\right] \tag{9}$$

$$k_1 = \begin{cases} 1 & if\ min\left[\frac{e_2}{d_o}; \frac{p}{2d_o}\right] > 1.5 \\ 0.8 & if\ min\left[\frac{e_2}{d_o}; \frac{p}{2d_o}\right] \leq 1.5 \end{cases} \tag{10}$$

4.4 | AISC 370

The American standard AISC 370 [13] serves as the reference standard for the design of stainless steel bolted connections. Similar to EC3-1-8 [12] and EC3-1-4 [20], it provides a series of equations to estimate the failure capacity of shear bolted

TABLE 5 | Estimated failure mechanisms and load capacity ratios for single-bolt configurations using LBE [5, 22].

Designation	Design resistance to LBE, F_{LBE} (kN)	Ratio to LBE, $\frac{F_{Exp}}{F_{LBE}}$	Failure mode (F_{LBE})
IP1-1-CO	20.3	0.93	SO
IP1-1-WAAM-M-0°	15.8	1.16	SO
IP1-1-WAAM-M-45°	16.8	1.14	SO
IP1-1-WAAM-M-60°	16.1	1.15	SO
IP1-1-WAAM-M-90°	17.1	1.04	SO
IP1-1-WAAM-AB-0°	40.1	1.10	SO
IP1-1-SLM-M-0°	19.1	0.97	SO
IP1-1-SLM-AB-0°	19.1	0.98	SO
IP1-2-CO	18.8	0.96	SO
IP1-2-WAAM-M-0°	14.7	1.15	SO
IP1-2-WAAM-M-45°	15.5	1.23	SO
IP1-2-WAAM-M-60°	14.9	1.21	SO
IP1-2-WAAM-M-90°	15.8	1.03	SO
IP1-2-WAAM-AB-0°	37.0	1.10	SO
IP1-2-WAAM-AB-45°	40.1	1.04	SO
IP1-2-WAAM-AB-60°	40.9	0.93	SO
IP1-2-WAAM-AB-90°	35.7	1.17	SO
IP1-2-SLM-AB-0°	17.6	1.04	SO
IP1-2-SLM-AB-45°	15.8	1.18	SO
IP1-2-SLM-AB-90°	15.6	1.12	SO
IP1-3-CO	15.7	1.00	SO
IP1-3-WAAM-M-0°	12.3	1.22	SO
IP1-3-WAAM-AB-0°	30.2	1.11	SO
IP1-4-CO	11.0	1.03	SO
IP1-4-WAAM-M-0°	8.6	1.30	SO
IP1-4-WAAM-AB-0°	21.0	1.13	SO

connections, but with different coefficient values depending on the adopted design criterion. The bearing resistance, $F_{b,AISC370}$ is determined using Equation (11), where the coefficient C_b is taken as 2.5 for $l_2/d_o > 1.5$ or 2 for $l_2/d_o \leq 1.5$. Here, the parameter l_2 is the distance from the center of the hole to the center of the adjacent hole or the edge of the plate perpendicular to the direction of the applied load.

$$F_{b,AISC370} = n_b C_b f_u dt \tag{11}$$

Equation (12) defines the net-section tension design resistance, $F_{t,AISC370}$. It follows the same formulation as that in EC3-1-8 [12] with slight modification, as it does not account for the effect of the fabrication method. The values of $N_{pl,AISC370}$ and $N_{n,AISC370}$ are calculated using Equations (13), and (14), respectively.

$$F_{t,AISC370} = min\left[F_{pl,AISC370}; F_{n,AISC370}\right] \tag{12}$$

$$F_{pl,AISC370} = A_g f_y \tag{13}$$

$$F_{n,AISC370} = A_{net} f_u \tag{14}$$

For the design resistance against block tearing, $F_{eff,AISC370}$, Equation (15) shows that AISC 370 [13] adopts the same formulation as EC3-1-8 [12], except for a constant factor, which is 0.6 in AISC 370 [13], resulting in a slight variation in the estimated capacity.

$$F_{eff,AISC370} = \left[\left(A_{nt} f_u\right) + min\left(0.6A_{gv} f_y; 0.6A_{nv} f_u\right)\right] \tag{15}$$

Unlike EC3-1-8 [12] and EC3-1-4 [20], AISC370 [13] provides an explicit equation to estimate the design capacity estimation for shear-out failure, $F_{so,AISC370}$ given in Equation (16). The coefficients (C_t) and (C_h) are 2.5 and 3, respectively, under the strength criterion. The parameter l_1 refers to the distance from the center of the hole to the center of the adjacent hole or the edge of the plate parallel to the force.

$$F_{so,AISC370} = n_b C_t f_u dt\left(\frac{l_1}{C_h d_o}\right) \tag{16}$$

4.5 | Literature-Based Equations (LBE)

The previously mentioned study [8], which investigated 316L stainless steel double-lap shear bolted connections, demonstrated that applying the shear-out and bearing resistance equations originally formulated by [21, 22], respectively, yielded more accurate estimations than those obtained from codified design equations, with a reported mean estimation ratio of 1.06 and a coefficient of variation (COV) of 0.088. Subsequent work [23] introduced a modification to the shear-out equation to account for the bolt diameter, which was further refined by [5] to incorporate the effects of WAAM-produced carbon steel plates. Accordingly, the shear-out equation adopted in this study is that of [5], presented in Equation (17). The term l_{av} representing the length of active shear-out, is calculated using Equation (18), where l_c is the distance from the hole edge to the plate edge. The bearing resistance equation used remains that of [22], shown in

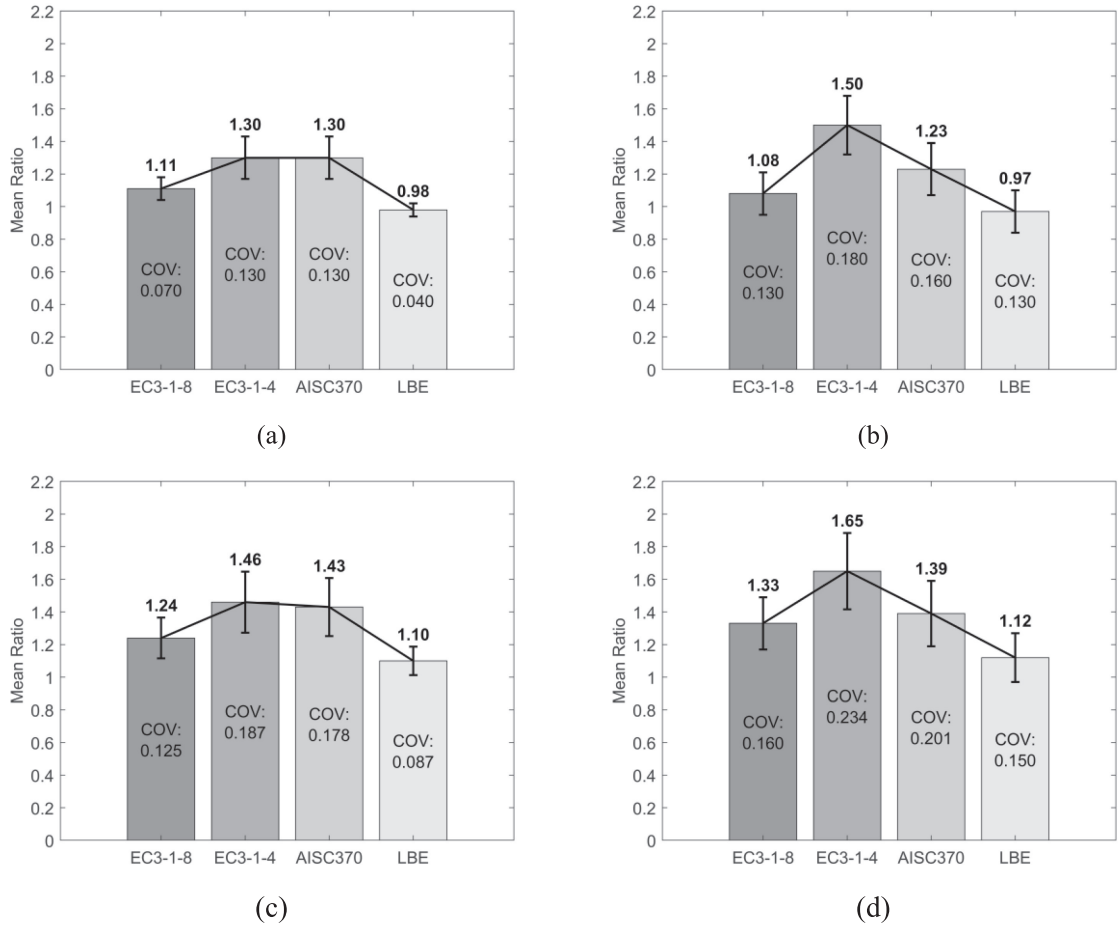

FIGURE 7 | Comparison of design provisions [12, 13, 20] and LBE [5, 22] estimations against experimental load capacity plates: mean ratios and COV of CON plates in (a) single-bolt and (b) double-bolt configurations and for AM plates in (c) single-bolt and (d) double-bolt configurations.

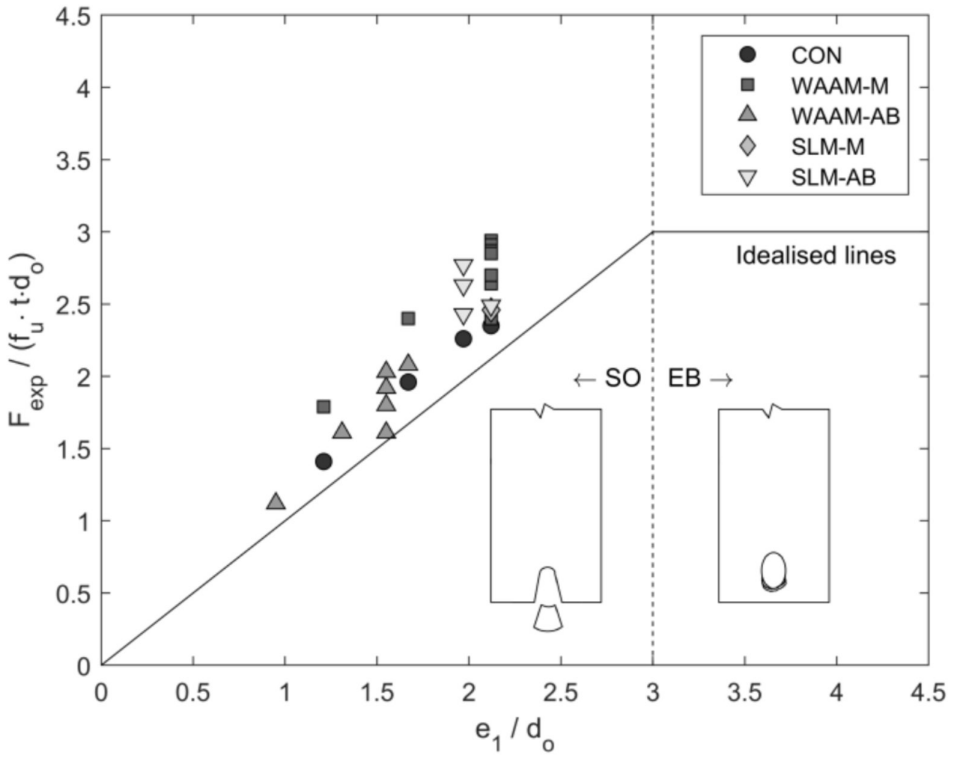

FIGURE 8 | Indirect interpretation of EC3-1-8 [12] showing the threshold between EB and SO governing failures for single-bolted configurations connection results, using the condition $e_1 / d_o < 3$ as derived from the definition of a_b in [5].

TABLE 6 | Comparison between experimental results and design provision estimations [12, 13, 20] for the failure mechanisms of double-bolt configurations.

Designation	Experimental ultimate load, F_{Exp} (kN)	Governing failure mode	Design resistance to EC3-1-8, $F_{EC3-1-8}$ (kN)	Ratio to EC3-1-8, $\frac{F_{Exp}}{F_{EC3-1-8}}$	Failure mode (EC3-1-8)	Design resistance to EC3-1-4, $F_{EC3-1-4}$ (kN)	Ratio to EC3-1-4, $\frac{F_{Exp}}{F_{EC3-1-4}}$	Failure mode (EC3-1-4)	Design resistance to AISC370, $F_{AISC370}$ (kN)	Ratio to AISC370, $\frac{F_{Exp}}{F_{AISC370}}$	Failure mode (AISC370)
IP2-1-CON	27.3	BT*	25.9	1.05	BT	19.4	1.41	EB	24.3	1.12	SO
IP2-1-WAAM-M-0°	26.3	BT*	17.8	1.48	BT	15.2	1.73	EB	18.1	1.45	BT
IP2-1-WAAM-M-45°	27.4	BT*	19.4	1.41	BT	16.1	1.70	EB	19.7	1.39	BT
IP2-1-WAAM-M-60°	26.8	BT*	18.2	1.47	BT	15.4	1.74	EB	18.5	1.45	BT
IP2-1-WAAM-M-90°	25.3	BT*	18.4	1.38	BT	16.3	1.55	EB	18.7	1.35	BT
IP2-2-CON	26.6	BT	24.4	1.09	BT	17.8	1.49	EB	22.2	1.20	SO
IP2-2-WAAM-M-0°	27.3	BT	17.1	1.60	BT	13.9	1.96	EB	17.4	1.57	SO+BT
IP2-2-WAAM-AB-0°	57.0	BT	40.0	1.43	BT	37.9	1.50	EB	42.6	1.34	BT
IP2-3-CON	23.1	SO	19.9	1.16	EB	13.3	1.74	EB	16.6	1.39	SO
IP2-3-WAAM-M-0°	23.8	SO	15.2	1.57	BT	10.4	2.29	EB	12.9	1.84	SO
IP2-3-WAAM-M-45°	24.4	BT	16.5	1.48	EB + BT	11.0	2.22	EB	13.7	1.78	SO
IP2-3-WAAM-M-60°	23.3	BT	15.6	1.49	BT	10.5	2.22	EB	13.2	1.77	SO
IP2-3-WAAM-M-90°	21.6	BT	15.9	1.36	BT	11.2	1.93	EB	12.3	1.76	SO
IP2-3-WAAM-AB-0°	49.5	BT	33.7	1.47	BT	28.7	1.72	EB	34.2	1.45	BT
IP2-3-WAAM-AB-45°	47.7	BT	34.6	1.38	BT	29.9	1.60	EB	35.1	1.36	BT

(Continues)

TABLE 6 | (Continued)

Designation	Experimental ultimate load, F_{Exp} (kN)	Governing failure mode	Design resistance to EC3-1-8, $F_{EC3-1-8}$ (kN)	Ratio to EC3-1-8, $\frac{F_{Exp}}{F_{EC3-1-8}}$	Failure mode (EC3-1-8)	Design resistance to EC3-1-4, $F_{EC3-1-4}$ (kN)	Ratio to EC3-1-4, $\frac{F_{Exp}}{F_{EC3-1-4}}$	Failure mode (EC3-1-4)	Design resistance to AISC370, $F_{AISC370}$ (kN)	Ratio to AISC370, $\frac{F_{Exp}}{F_{AISC370}}$	Failure mode (AISC370)
IP2-3-WAAM-AB-60°	48.9	SO	38	1.29	BT	30.4	1.61	EB	38.6	1.27	BT
IP2-3-WAAM-AB-90°	44.9	BT	31.9	1.41	BT	27.2	1.65	EB	32.4	1.39	BT
IP2-4-CON	23.0	BT	19.4	1.19	EB	12.9	1.78	EB	16.2	1.42	SO
IP2-4-WAAM-M-0°	23.1	SO	15.1	1.53	BT	10.1	2.29	EB	12.6	1.83	SO
IP2-4-WAAM-AB-0°	47.6	BT	29.6	1.61	BT	25.0	1.90	EB	30.0	1.59	BT
IP2-5-CON	21.1	SO	17.0	1.24	EB	11.3	1.87	EB	14.1	1.50	SO
IP2-5-WAAM-M-0°	20.7	SO	13.3	1.56	EB	8.8	2.35	EB	11.1	1.86	SO
IP2-5-WAAM-AB-0°	43.7	SO	28.3	1.54	BT	23.2	1.88	EB	28.6	1.53	BT
IP2-6-CON	30.4	NST*	35.8	0.85	NST	25.9	1.17	EB	32.0	0.95	EB
IP2-6-WAAM-AB-0°	70.8	NST*	60.0	1.18	NST	54.1	1.31	EB	60.0	1.18	NST
IP2-6-WAAM-AB-45°	62.8	NST*	56.4	1.11	NST	55.3	1.14	EB	56.4	1.11	NST
IP2-6-WAAM-AB-60°	61.8	NST*	68.4	0.90	NST	60.9	1.01	EB	68.5	0.90	NST
IP2-6-WAAM-AB-90°	61.7	NST*	54.6	1.13	NST	50.1	1.23	EB	54.6	1.13	NST
IP2-6-SLM-AB-0°	31.1	NST*	33.6	0.93	NST	24.3	1.28	EB	30.1	1.03	EB
IP2-6-SLM-AB-45°	31.6	NST*	30.1	1.05	NST	21.8	1.45	EB	27.0	1.17	EB

(Continues)

TABLE 6 | (Continued)

Designation	Experimental ultimate load, F_{Exp} (kN)	Governing failure mode	Design resistance to EC3-1-8, $F_{EC3-1-8}$ (kN)	Ratio to EC3-1-8, $\frac{F_{Exp}}{F_{EC3-1-8}}$	Failure mode (EC3-1-8)	Design resistance to EC3-1-4, $F_{EC3-1-4}$ (kN)	Ratio to EC3-1-4, $\frac{F_{Exp}}{F_{EC3-1-4}}$	Failure mode (EC3-1-4)	Design resistance to AISC370, $F_{AISC370}$ (kN)	Ratio to AISC370, $\frac{F_{Exp}}{F_{AISC370}}$	Failure mode (AISC370)
IP2-6-SLM-AB-90°	30.6	NST*	29.7	1.03	NST	21.5	1.42	EB	26.6	1.15	EB
IP2-7-CON	32.1	BT*	32.1	1.00	BT	30.3	1.06	EB	30.3	1.06	SO
IP2-7-WAAM-M-0°	31.4	BT*	21.9	1.43	BT	21.9	1.43	BT	22.2	1.41	BT
IP2-7-WAAM-AB-0°	69.1	NST	51.6	1.34	BT	51.6	1.34	BT	52.6	1.31	BT
IP2-7-SLM-M-0°	31.7	BT*	31.2	1.02	BT	28.5	1.11	EB	31.9	0.99	BT
IP2-7-SLM-AB-0°	33.5	BT*	31.2	1.07	BT	28.5	1.18	EB	31.9	1.05	BT

Abbreviations: BT* = partial block tearing; NST* = partial net-section tension.

Equation (19). The LBE final load estimations, denoted as F_{LBE}, were used for all specimens except those designed with variations in geometric parameters e_2 and p, as the equations do not account for these changes [5, 22].

$$F_{s,Guo} = 1.2 n_b l_{av} t f_u \left(\frac{3d}{e_1}\right)^{0.1} \tag{17}$$

$$l_{av} = l_c + \frac{d_o}{4} \tag{18}$$

$$F_{b,\ Teh\&Uz} = 3.5 n_b d t f_u \tag{19}$$

The aforementioned equations were specifically selected due to their refined formulations, enhancing the accuracy of estimating the failure mechanisms for WAAM-produced plates. Moreover, the selected equations are considered potentially suitable for estimating failures in SLM-produced specimens.

4.6 | Results and Discussion

The design provisions [12, 13, 20] and LBE [5, 22] estimations for single-bolted configurations are summarized in Tables 4 and 5, noting that inner plates governed by NST failures were excluded from these LBE estimations, since the equations are not defined for this mode. Figure 7a,c compares the experimental-to-estimated failure load ratios for CON and AM plates in the single-bolted configuration, showing a reduced variability of the ratios for CON plates. The most conservative results were from standards specifically tailored to stainless steel, with peak ratios of experimental-to-estimated failure loads reaching 1.85 in EC3-1-4 [20] and 1.78 under AISC 370 [13], indicating a pronounced tendency toward overdesign. Conversely, EC3-1-8 [12] provided more accurate estimations. This may reflect the more generalized nature of the bearing resistance equation adopted from EC3-1-8 [12], which, despite being developed for carbon steel, appears to align more closely with the load-bearing response of the AM plates. The LBE [5, 22] estimations, primarily governed by SO failures, yielded the most accurate results, as clearly illustrated in Figure 7c. The mean ratio of experimental-to-estimated failure loads obtained from LBE estimations for AM plates was 1.10, accompanied by a low coefficient of variation (COV) of 0.087. This finding aligns closely with the observations reported in [8]. In contrast, AISC 370 [13] showed the highest mean ratio and variability, with values of 1.43 and 0.178, respectively. Furthermore, most observed failures involved a governing SO failure, which in EC3-1-8 [12] and EC3-1-4 [20], is accounted for under the bearing resistance check, where capacity decreases with reducing e_1 and therefore their estimations correspond to EB, whereas AISC 370 [13] includes an explicit shear-out resistance equation. As shown in Figure 8, the distinction between EB and SO can be illustrated using the $e_1 / d_o < 3$ condition derived from the definition of a_b in [5], which interpreted SO in EC3-1-8 [12] as being covered by the bearing resistance check. However, since stainless steel ductility makes the plate tend to have a mix of both failures, this approach provides a clarification on whether SO will occur to plates after the initial EB failure. This is why it was mentioned earlier that the failure is EB + SO with SO governing.

For double-bolted configurations, Tables 6 and 7 present the corresponding design provisions [12, 13, 20] and LBE [5, 22]

TABLE 7 | Estimated failure mechanisms and load capacity ratios for double-bolt configurations using LBE [5, 22].

Designation	Design resistance to LBE, F_{LBE} (kN)	Ratio to LBE, $\frac{F_{Exp}}{F_{LBE}}$	Failure mode (F_{LBE})
IP2-1-CON	34.5	0.79	SO
IP2-1-WAAM-M-0°	27.0	0.97	SO
IP2-1-WAAM-M-45°	28.6	0.96	SO
IP2-1-WAAM-M-60°	27.4	0.98	SO
IP2-1-WAAM-M-90°	29.1	0.87	SO
IP2-2-CON	31.4	0.85	SO
IP2-2-WAAM-M-0°	24.6	1.11	SO
IP2-2-WAAM-AB-0°	62.6	0.91	SO
IP2-3-CON	22.7	1.02	SO
IP2-3-WAAM-M-0°	17.7	1.34	SO
IP2-3-WAAM-M-45°	18.8	1.30	SO
IP2-3-WAAM-M-60°	18.0	1.29	SO
IP2-3-WAAM-M-90°	19.1	1.13	SO
IP2-3-WAAM-AB-0°	45.0	1.10	SO
IP2-3-WAAM-AB-45°	46.1	1.03	SO
IP2-3-WAAM-AB-60°	50.7	0.96	SO
IP2-3-WAAM-AB-90°	42.6	1.05	SO
IP2-4-CON	22.0	1.05	SO
IP2-4-WAAM-M-0°	17.2	1.34	SO
IP2-4-WAAM-AB-0°	39.0	1.22	SO
IP2-5-CON	18.8	1.12	SO
IP2-5-WAAM-M-0°	14.7	1.41	SO
IP2-5-WAAM-AB-0°	34.8	1.26	SO

estimations. Similar to the single-bolted configurations, specimens governed by NST failures were excluded from the LBE [5, 22] estimations. Given the complexity introduced by the interaction of two bolt holes, significant variability was noted in the ratios for EC3-1-4 [20] and AISC 370 [13], with mean ratios of 1.65 and 1.39 and respective COV values of 0.234 and 0.201 (Figure 7d). The design standard EC3-1-8 [12] exhibited lower mean ratios (1.33) and reduced variability (COV = 0.160) compared to EC3-1-4 [20] yet still demonstrated considerable conservatism. The LBE [5, 22] estimations again proved the most accurate, yielding a mean ratio of 1.12. However, the higher COV of 0.150 reflects a modest reduction in consistency compared to the single-bolted results. For CON plates, the corresponding double-bolt configuration results (Figure 7b) show improved agreement and lower scatter relative to AM plates, although EC3-1-4 [20] still leads to pronounced conservatism. The associated failure modes of the double-bolted configurations were not consistently captured by the design standards [12, 13, 20] or the LBE [5, 22], with several cases showing clear discrepancies between predicted and observed modes. In particular, EC3-1-4 [20] predominantly predicted EB, while the governing failures were SO, NST, and BT. Since the LBE [5, 22] equations are defined only for SO and EB, all cases of BT were predicted as SO.

Collectively, these results highlight the significant conservatism inherent in current stainless steel-specific design provisions when applied to WAAM and SLM-produced plates in bolted connections, while their application to CON plates remains generally reliable and conservative. The consistent accuracy and lower variability of the LBE [5, 22] estimations suggest that these equations, explicitly formulated for AM, are more suitable than traditional, generalized stainless steel guidelines. This implies that current design codes may require calibration or the introduction of appropriate adjustment factors to adequately capture the unique mechanical response of WAAM and SLM fabricated components, achievable through further experimental and numerical research on AM bolted connections.

5 | Conclusions

The global load–displacement comparisons between CON and AM plates, together with the evaluation of load capacities against design provisions and LBE estimations for hybrid double-lap shear connections, led to the following conclusions:

- Bolted connections with integrated AM inner plates exhibited lower displacement at failure compared to CON plates, indicating noticeably reduced ductility and elongation capacity across both single- and double-bolt configurations, despite no significant differences in load capacity. Therefore, special attention should be given to the design of connections to ensure a ductile and thus safe structural response.
- The increased thickness in WAAM-AB plates significantly enhanced load-bearing capacity, highlighting the dominant role of thickness in structural performance, even when surface undulations exist that cause local variation in thickness.
- The diagonal extraction orientation clearly enhanced ductility in both WAAM-M and WAAM-AB plates, demonstrating its beneficial effect.
- Design codes tailored to stainless steel, such as EC3-1-4 [20] and AISC 370 [13], were overly conservative, especially in

AM applications, with high experimental-to-estimated failure loads mean ratios and COVs suggesting potential for overdesign and inefficiency.

- EC3-1-8 [12], although developed for carbon steel, performed better for AM plates due to its more generalized formulation, specifically in the bearing resistance equation, producing closer estimations with reduced variability in both single- and double-bolt configurations.
- For CON plates, the assessed design standards generally provided conservative estimations, with ratios closer to unity and lower variability than those for AM plates.
- LBE [5, 22] consistently outperformed code provisions, showing the lowest deviation from experimental results and offering more accurate load capacity estimations.
- Current design standards inadequately estimate the failure mechanisms in AM plates, underlining the need for updated equations or modification factors based on experimental and numerical data tailored to WAAM and SLM plates' specific behavior.

Author Contributions

Hasan Almuhanna: writing – original draft, investigation, formal analysis. **Giacomo Torelli:** writing – review and editing, supervision. **Luca Susmel:** writing – review and editing, supervision, methodology, conceptualization.

Acknowledgments

This work was supported by the Henry Royce Institute for Advanced Materials, funded through EPSRC grants EP/R00661X/1, EP/P025021/1, and EP/S019367/1. The authors would also like to acknowledge the Kuwait Institute for Scientific Research (KISR) for funding the tuition fees of the lead author's PhD program.

Conflicts of Interest

The authors declare no conflicts of interest.

Data Availability Statement

Data will be made available on request.

References

1. G. Liu, X. Zhang, X. Chen, et al., "Additive Manufacturing of Structural Materials," *Materials Science & Engineering R: Reports* 145 (2021): 100596, https://doi.org/10.1016/j.mser.2020.100596.

2. L. Gardner, P. Kyvelou, G. Herbert, and C. Buchanan, "Testing and Initial Verification of the World's First Metal 3D Printed Bridge," *Journal of Constructional Steel Research* 172 (2020):106233, https://doi.org/10.1016/j.jcsr.2020.106233.

3. L. Gardner, "Metal Additive Manufacturing in Structural Engineering—Review, Advances, Opportunities and Outlook," *Structure* 47 (2023): 2178–2193, https://doi.org/10.1016/j.istruc.2022.12.039.

4. X. Guo, P. Kyvelou, J. Ye, L. H. Teh, and L. Gardner, "Experimental Investigation of Wire Arc Additively Manufactured Steel Single-Lap Shear Bolted Connections," *Thin-Walled Structures* 181 (2022): 110029, https://doi.org/10.1016/j.tws.2022.110029.

5. X. Guo, P. Kyvelou, J. Ye, L. H. Teh, and L. Gardner, "Experimental Study of DED-Arc Additively Manufactured Steel Double-Lap Shear Bolted Connections," *Engineering Structures* 281 (2023): 115736, https://doi.org/10.1016/j.engstruct.2023.115736.

6. Y. Liu, J. Ye, Y. Yang, et al., "Experimental Study on Wire and Arc Additively Manufactured Steel Double-Shear Bolted Connections," *Journal of Building Engineering* 76 (2023): 107330, https://doi.org/10.1016/j.jobe.2023.107330.

7. Y. Liu, J. Ye, J. He, et al., "Testing and Design of Wire and Arc Additively Manufactured Steel Double-Shear Bolted Connections With Thick Plates," *Journal of Constructional Steel Research* 224 (2025): 109069, https://doi.org/10.1016/j.jcsr.2024.109069.

8. W. Zuo, M. T. Chen, S. W. Liu, et al., "Experimental Investigation on Double-Lap Shear Behavior of 3D Printed Austenitic Stainless Steel Bolted Connections," *Engineering Structures* 317 (2024): 118501, https://doi.org/10.1016/j.engstruct.2024.118501.

9. W. Zuo, M. T. Chen, O. Zhao, et al., "Behavior of Wire Arc Additively Manufactured 316L Austenitic Stainless Steel Single Shear Bolted Connections," *Thin-Walled Structures* 202 (2024): 112075, https://doi.org/10.1016/j.tws.2024.112075.

10. W. Zuo, M. T. Chen, O. Zhao, et al., "Structural Performance of Wire Arc Additively Manufactured Duplex Stainless Steel Single-Lap Shear Bolted Connections," *Engineering Structures* 319 (2024): 118706, https://doi.org/10.1016/j.engstruct.2024.118706.

11. BS EN 1993-1-8, "Eurocode 3 Design of Steel Structures—Part 1–8 Design of Joints," 2021.

12. BS EN 1993-1-8, "Eurocode 3. Design of Steel Structures. Part 1–8: Joints," 2024.

13. ANSI/AISC 370, "Specification for Structural Stainless Steel Buildings," 2021.

14. F. Bartolomeu, M. Buciumeanu, E. Pinto, et al., "316L Stainless Steel Mechanical and Tribological Behavior—A Comparison Between Selective Laser Melting, Hot Pressing and Conventional Casting," *Additive Manufacturing* 16 (2017): 81–89, https://doi.org/10.1016/j.addma.2017.05.007.

15. D. Yang, X. Kan, P. Gao, Y. Zhao, Y. Yin, et al., "Influence of Porosity on Mechanical and Corrosion Properties of SLM 316L Stainless Steel," *Applied Physics A: Materials Science & Processing* 128 (2022): 51 https://doi.org/10.1007/s00339-021-05191-4.

16. M. Sanjari, M. Mahmoudiniya, H. Pirgazi, et al., "Microstructure, Texture, and Anisotropic Mechanical Behavior of Selective Laser Melted Maraging Stainless Steels," *Materials Characterization* 192 (2022): 112185, https://doi.org/10.1016/j.matchar.2022.112185.

17. X. q. Ni, D. c. Kong, Y. Wen, et al., "Anisotropy in Mechanical Properties and Corrosion Resistance of 316L Stainless Steel Fabricated by Selective Laser Melting," *International Journal of Minerals, Metallurgy, and Materials* 26 (2019): 319–328, https://doi.org/10.1007/s12613-019-1740-x.

18. Z. Kong, R. Li, X. Wang, et al., "Shear Capacity of Additively Manufactured Stainless Steel Bolted Connections After Fire," *Engineering Structures* 322 (2025): 119102, https://doi.org/10.1016/j.engstruct.2024.119102.

19. H. Almuhanna, G. Torelli, R. Kindermann, and L. Susmel, "Failure Investigation of Hybrid Double-Lap Shear Bolted Connections With Additively Manufactured 316L Stainless Steel Inner Plates," *Engineering Failure Analysis* 179 (2025): 109756, https://doi.org/10.1016/J.ENGFAILANAL.2025.109756.

20. BS EN 1993-1-4, "Eurocode 3. Design of Steel Structures. Part 1–4: Stainless Steel Structures," 2025.

21. L. H. Teh and M. E. Uz, "Ultimate Shear-Out Capacities of Structural-Steel Bolted Connections," *Journal of Structural Engineering* 141 (2015): 04014152, https://doi.org/10.1061/(asce)st.1943-541x.0001105.

22. L. H. Teh and M. E. Uz, "Combined Bearing and Shear-Out Capacity of Structural Steel Bolted Connections," *Journal of Structural*

Engineering 142 (2016), https://doi.org/10.1061/(asce)st.1943-541x.0001573.

23. H. Xing, L. H. Teh, Z. Jiang, and A. Ahmed, "Shear-Out Capacity of Bolted Connections in Cold-Reduced Steel Sheets," *Journal of Structural Engineering* 146 (2020): 04020018, https://doi.org/10.1061/(asce)st.1943-541x.0002565.